



# Benchmarking the Swedish Power Grid Against a 1-in-100-Year Geoelectric Field Scenario

Vanina Lanabere<sup>1</sup>, Andrew P. Dimmock<sup>1</sup>, Sven Molenkamp Venholen<sup>2</sup>, Alice Wallner<sup>1,3</sup>, Andreas Johlander<sup>2</sup>, Lisa Rosenqvist<sup>2</sup>, and Johan Setréus<sup>4</sup>

**Correspondence:** Vanina Lanabere (vanina.lanabere@irfu.se)

Abstract. Sweden's communication and power systems have been impacted by extreme space weather events in the past. For instance, the May 1921 storm caused a fire at the telegraph and telephone station in Karlstad, and the 2003 Halloween storm led to a blackout in Malmö. In this study, we present the first comprehensive assessment of the potential impacts of a 1-in-100-year event on the entire Swedish power grid. Using magnetic field observations from the 30 October 2003 event as a baseline, we constructed two extreme scenarios. In Case 1, we used the observed magnetic field across Fennoscandia. In Case 2, we assume a spatially uniform ionospheric current system, producing identical magnetic waveforms across the country. Then the estimated 3D electric field was scaled using region-specific scaling factors derived from recent statistical analyses of electric field extremes in Sweden. The scaled geoelectric field and power lines voltages are computed using the recently developed RAISE model, which includes realistic ground conductivity and power line topology. Our results show that the strongest horizontal electric fields, around 12 V/km, occur within the 55° and 58° MLAT band, particularly in regions with sharp lateral conductivity gradients. East—west-oriented power lines are especially vulnerable, as they align with the dominant orientation of the induced electric field. Overall, during the peak of a 1-in-100-year geomagnetic storm, more than 100 transmission lines are expected to experience voltages above 50 V multiple times over the course of the substorm. At the peak of the strongest disturbance, triggered by a sudden weakening of the westward electrojet, around 100 lines are expected to exceed 100 V. These results provide critical insights into infrastructure vulnerability under extreme space weather.

# 1 Introduction

The vulnerability of modern infrastructure to extreme space weather events is an increasing concern, given society's growing dependence on reliable electrical and communication systems. Power transmission grids are particularly at risk from geomagnetically induced currents (GICs), which are driven by rapid variations in the geomagnetic field during geomagnetic storms. These currents can disrupt normal grid operations and, in extreme cases, cause permanent transformer damage or trigger widespread, unnecessary tripping of both power lines and transformers, potentially resulting in large-scale power outages (e.g., Bolduc, 2002; Pulkkinen et al., 2005). While ground magnetic field perturbations (dB/dt) are often used as proxies for GIC

<sup>&</sup>lt;sup>1</sup>Swedish Institute of Space Physics, Uppsala, Sweden

<sup>&</sup>lt;sup>2</sup>Swedish Defence Research Agency, Stockholm, Sweden

<sup>&</sup>lt;sup>3</sup>Department of Physics and Astronomy, Uppsala University, Uppsala, Sweden

<sup>&</sup>lt;sup>4</sup>Swedish National Grid-Svenska Kraftnät, Sundbyberg, Sweden





activity (Viljanen et al., 2001), the horizontal geoelectric field ( $E_H$ ) is a more direct and physically meaningful driver, as it incorporates the effects of local ground conductivity (Pulkkinen et al., 2017). Consequently, several statistical studies have examined extreme geoelectric field values in different areas, including Canada (Cordell et al., 2025), Ireland (Malone-Leigh et al., 2024), and Sweden (Lanabere et al., 2023; Lanabere et al., 2024). Although extreme events are typically low-probability but high-impact, it remains essential to define what constitutes an extreme event in order to benchmark worst-case scenarios.

A worst-case scenario is typically defined as an event with an occurrence rate of 1-in-100 years (Pulkkinen et al., 2012). The global level of geomagnetic activity is most commonly quantified using the Dst index. The most extreme value inferred to date is associated with the Carrington event (Carrington, 1859), with estimates ranging from approximately -850 to -1760 nT (Siscoe et al., 2006; Tsurutani et al., 2003). Although the exact recurrence rate of such an extreme event remains uncertain, recent statistical analyses suggest a return period on the order of 1000 years, with confidence intervals ranging from approximately 400 to 2800 years (Love et al., 2024). Another event exceeding the 1-in-100 year threshold (Bergin et al., 2023) was the May 1921 storm, with an estimated Dst of about -900 nT (Kappenman, 2006; Hapgood, 2019). The next largest event was the March 1989 storm (Dst  $\sim$ -589 nT), which has an estimated occurrence rate of about 1 in 60 years (Tsubouchi and Omura, 2007) to 1 in 100 years according to Bergin et al. (2023). However, these earlier events were poorly documented due to limited observational coverage at the time. The first well-recorded extreme geomagnetic storm was the Halloween event of 29–30 October 2003, which reached a minimum Dst of approximately -400 nT. More recently, the storm of 10–12 May 2024 reached a minimum Dst of about -412 nT, making it the most severe geomagnetic storm since the Halloween storms of 2003 and the second largest event after the 13 March 1989 storm.

Previous worst-case studies have used the records of the latest geomagnetic storms to reconstruct 1-in-100 years scenarios for the geoelectric field event (Pulkkinen et al., 2012; Ngwira et al., 2013). Other studies, however, have adopted alternative approaches by scaling the geomagnetic field (NERC, 2016), and the magnetic field perturbation (Mac Manus et al., 2022) into a 1-in-100 years scenarios. In order to scale the electric field, magnetic field, or its perturbation, the mentioned authors have used different scaling methods to account for the maximum intensity and return values dependence with magnetic latitude (MLAT). Then, the MLAT threshold of the extreme events becomes an important factor. For instance, Pulkkinen et al. (2012) analyzed two extreme geomagnetic storms, and proposed that major disturbances typically occur near 50° MLAT. Later, Ngwira et al. (2013) extended the study to twelve severe geomagnetic storm events and found that the latitude threshold boundary tends to occur between 50° and 55° MLAT. Regionally, Thomson et al. (2011) analyzed 28 years of European geomagnetic data and observed a local maximum around 53–62° MLAT for the time derivative of the horizontal magnetic field. This result is consistent with the findings of Lanabere et al. (2023), who showed that 58.7° MLAT had the highest frequency of the 15 largest events observed between 2000 and 2018. Additionally, the largest electric field values in Sweden are expected to occur around 56.9° MLAT, according to (Lanabere et al., 2024).

The first worst-case scenario study for Sweden was conducted by Rosenqvist et al. (2022), who analyzed the ground magnetic response to a modeled "perfect" storm. Due to the current models limitations to fully capture the complexity of substorm dynamics, Rosenqvist et al. (2022) focused their analysis on magnetic field variations during the sudden impulse phase to predict a worst-case GIC magnitude for a power line in southern Sweden. However, large amplitude dB/dt are typically





attributed to substorms (Viljanen et al., 2006; Kataoka and Ngwira, 2016) which are responsible of the largest  $E_H$  values estimated in Sweden (Lanabere et al., 2023). Thus, the impact of a 1-in-100-year event, associated with nightside events on Sweden's power grid remains largely uncertain.

This paper extends the work of Rosenqvist et al. (2022) by analyzing ground magnetic data during the development of a premidnight substorm event. Following the approach of Pulkkinen et al. (2012), we define an extreme event as the 100-year maximum amplitude of the  $E_H$  at 10-second resolution. The remainder of the paper of this paper is organized as follows. Section 2 describes the geomagnetic field data, the GIC-SMAP model developed by Rosenqvist and Hall (2019) to estimate the geoelectric field in Sweden, and the RAISE model (Rosenqvist et al., 2025), used to simulate the resulting power line voltages in the Swedish power grid under the scaled electric field. In Section 3, we describe the selection of geomagnetic field observations from a past storm, and the application of scaling factors from Lanabere et al. (2024) to represent a once in 100 year event. In Section 4, we evaluate the impacts of the scaled geoelectric field on the power grid. Finally, Section 5 and 6 presents the discussion and conclusions respectively.

#### 70 2 Data and models

This study relies on the availability of magnetic field measurements in the Fennoscandia region for a previous severe event. In a previous study, Lanabere et al. (2023) identified the event on 30 October 2003 at 20:03:40  $\pm$  1 hour as the event with largest 1D geoelectric field in Sweden ( $E_H=2.73~{\rm V/km}$ ) during the last two solar cycles. This finding was later confirmed by Rosenqvist et al. (2025), who reported the largest 3D geoelectric field ( $E_H=22.4~{\rm V/km}$ ) for the same event over the same period. The significantly higher value in Rosenqvist et al. (2025) is attributed to the fact that the maximum was observed near Sweden's west coast, an area not covered in the analysis by Lanabere et al. (2023). This was also the first strong and well-recorded geomagnetic storm in this region. Although the 10–12 May 2024 event was the second most intense geomagnetic storm, its impact on the  $E_H$  in Sweden was significantly smaller than the Halloween event (Rosenqvist et al., 2025). This was mainly because Sweden was located on the dayside during the strongest effects of the storm, underscoring that an extreme geomagnetic storm does not necessarily produce extreme conditions everywhere at the same time.

We used 10-s geomagnetic field data from the IMAGE (International Monitor for Auroral Geomagnetic Effects) magnetometer network. At the time of the Halloween storm in October 2003, 26 magnetometers were operational in the Fennoscandian region. The IMAGE magnetometer network has been used to compute the equivalent ionospheric currents, which represent the horizontal ionospheric currents that would be required to produce the observed ground magnetic variations (Amm, 1997). This approach is used to obtain the magnetic field all over Sweden. Moreover, since ground-based geomagnetic measurements include both external ( $B_{ext}$ ) produced by ionospheric and magnetospheric currents, and internal ( $B_{int}$ ) produced by induced telluric currents, the method has been further refined to separate these components, as described by Juusola et al. (2020). We refer the reader to Amm (1997) and Amm and Viljanen (1999) for a more detailed explanation of the ionospheric equivalent current technique and its applications.



100



Table 1. Workflow of the analysis steps used in this study.

Step	Description	Reference
1	Magnetic field input selection (spatially uniform and non-uniform magnetic field).	
2	Calculation of the geoelectric field over Sweden using the GIC-SMAP model.	Rosenqvist and Hall (2019)
3	Scaling of the electric field values according to geomagnetic latitude (MLAT) bands following	Lanabere et al. (2024)
4	Application of the scaled electric fields into the <b>RAISE model</b> to compute power line voltages.	Rosenqvist et al. (2025)

The recently developed RAISE model (Rymdvädersmodell för Analys av Inducerade Strömmar och Elektriska fält, Swedish for "Space Weather Model for the Analysis of Induced Currents and Electric Fields"), introduced by Rosenqvist et al. (2025), was employed to analyze the voltages in the Swedish power grid lines. The simplified Swedish power grid representation consists of 194 nodes and 335 transmission lines, of which 49% are 400 kV lines and 51% are 220 kV lines. This model has previously been applied to investigate GIC activity during the April 2023 and May 2024 geomagnetic storms (Dimmock et al., 2024; Rosenqvist et al., 2025). RAISE integrates the GIC-SMAP model (Rosenqvist and Hall, 2019) with a simplified representation of the Swedish high-voltage power grid, assuming constant earthing resistance and fixed line resistances for both 200 kV and 400 kV transmission lines. Due to this simplification in line resistances, the results presented here focus on calculated voltages without explicitly computing the corresponding GICs. The GIC-SMAP model calculates the three-dimensional geoelectric field in Sweden and has been validated against GIC measurements (Rosenqvist and Hall, 2019; Rosenqvist et al., 2022). It incorporates a detailed three-dimensional conductivity model of the Earth, based on a crustal conductivity map with surrounding oceans for the Fennoscandian Shield (SMAP) (Engels et al., 2002; Korja et al., 2002), as further described in (Rosenqvist and Hall, 2019).

## 3 Method for defining worst-case scenarios

In this study, we follow the approach of Pulkkinen et al. (2012), defining a worst-case scenario when the amplitude of the  $E_H$  reaches an amplitude that occurs once in 100 years. Table 1 summarizes the workflow of the analysis conducted in this study. Each step, from the selection of magnetic field inputs, the recreation of a 1-in-100 year  $E_H$  event, to the impact in the Swedish power grid, is listed along with the corresponding model and/or reference to previous studies.

In the first step, we used magnetic field data from the Halloween event. The  $E_H$  reached during this event has been classified as having an estimated recurrence of 1-in-100-year event in northern Sweden, but only a 1-in-10- to 1-in-50-year event in southern Sweden (Lanabere et al., 2024). To gain a better understanding of a worst-case scenario, we explore two different scenarios. In the first case (Case 1), we use the actual observed magnetic field perturbation extrapolated to the whole Fennoscandian region. This approach is intended to capture a realistic situation where signatures of meso- and small-scale magnetosphere–ionosphere currents are represented. In the second case (Case 2), we construct an idealized scenario in which



125

130

135



**Table 2.** Scaling factors  $(S_f)$  applied to the horizontal geoelectric field  $(E_H)$  from the 30 October 2003 Halloween event to construct a physically plausible 1-in-100-year scenario across different geomagnetic latitude bands. Values based on the results of Lanabere et al. (2024)

MLAT range [°]	$S_f$
> 64	1.0
62–64	1.0
60–62	1.0
58-60	1.8
55–58	3.1
51–55	2.6

the magnetic field time series is spatially uniform across all magnetometer stations. Such a situation could be produced by a large-scale westward electrojet (WEJ) covering Fennoscandia, varying only in intensity. To represent this case, we use the  $B_{ext}$  from the SECS method, which reflects spatially and temporally varying ionospheric and magnetospheric currents.

In the second step, we applied the previously described GIC-SMAP model (Rosenqvist and Hall, 2019) to estimate the induced  $E_H$  in Sweden for the period 30 October 2003 between 19:40 to 20:30 UT, with a temporal resolution of 10 s. In Case 1, the  $E_H$  was estimated from the total magnetic field ( $B_{tot}$ ), whereas in Case 2 it was estimated from  $B_{ext}$ . Consequently,  $E_H$  will be underestimated in Case 2. However, using the external field allows estimation at locations where measurements were not collected, since it is independent of the ground conductivity.

The third step involves scaling the  $E_H$  to represent a worst-case scenario. To achieve this, a scaling factor ( $S_f$ ) is applied to generate a physically plausible 1-in-100-year event. By "plausible," we mean that the magnitude of the geoelectric field reaches its maximum near a characteristic geomagnetic latitude threshold. This threshold is generally expected to lie between  $53^{\circ}$  and  $62^{\circ}$  geomagnetic latitude, as suggested by Thomson et al. (2011). Then, we scaled the geoelectric field values by adopting the results from Lanabere et al. (2024), who estimated the 1-in-100 year return levels of the 1D geoelectric field at various locations in Sweden. Although these estimates are based on a 1D Earth conductivity model, the authors also provide normalized scaling factors relative to the peak electric field observed during the 2003 Halloween storm. In their results, the three northernmost sites exhibit return levels slightly below the October 2003  $E_H$  field peak, yet still within the 95 percent confidence interval. As a result, for these high-latitude locations, we adopt a conservative scaling factor of  $S_f = 1$ . The scaling factor varies with magnetic latitude, and the values in different magnetic latitude ranges are indicated in Table 2. We mention that we do not take into account the secular variation of the magnetic field, which is expected to show a great impact in Sweden since the change of the magnetic field during the last 40 years resulted in a shift toward lower latitudes.

Finally, in step four, the scaled  $E_H$  was used as input to the RAISE model (Rosenqvist et al., 2025) to compute the voltage time series for each of the 335 power grid lines. We report only the power line voltages, which represent the  $E_H$  integrated along the line's path, as the true line resistances required to estimate currents are considered sensitive information and a matter of national security. Assuming resistances to estimate currents would introduce additional uncertainty. Nevertheless, the total





voltages provide a valuable and meaningful metric for assessing the impact on the grid and can serve as a proxy for GICs, as they can later be converted to currents by the power grid operator.

#### 140 3.1 Case 1: Halloween geomagnetic storm

The magnetic field time series used in Case 1 are presented in Figure 1 and visualized in more detail in the animation Case1\_BE.mp4 (panels a,b,c), which consists of frames spanning 19:40 to 20:30 UT (50 minutes) with a 10-second timestep. Figure 1a shows the interpolated horizontal magnetic field component ( $\mathbf{B}_H$ ), based on data from the magnetic stations marked with black dots. The magnetic field components  $B_x$  and  $B_y$  time series are presented in Figure 1b,c. Around 19:47 UT, a local substorm onset occurred, marked by the initial drop in  $B_x$ , indicating the presence of a WEJ centered over the Fennoscandian region. During this period the WEJ peaked  $\sim$ 19:53:00–19:58:00 and  $\sim$ 20:02:00– 20:08:40 UT, which have been suggested to be caused by dipolarization of the nightside inner magnetosphere (Juusola et al., 2023). This is also observed in the  $B_H$  time series at the locations indicated by a star in Figure 1a, each location representing a different MLAT band in Sweden.  $B_x$  peaks around 19:56 in Northern Scandinavia ( $>60^\circ$  MLAT), few minutes later  $B_x$  peaks in central and Southern Scandinavia ( $54-60^\circ$  MLAT) around 20:04. Finally, a secondary  $B_x$  depression appeared at latitudes above  $60^\circ$  MLAT, followed by an abrupt weakening of  $B_x$  and a concurrent increase in  $B_y$  between 20:08 and 20:10 UT.

The maximum estimated  $E_H$  between 19:40 and 20:30 is summarized in Figure 2a, together with the  $E_H$  time series at the locations marked by stars Figure 2b,c. The maximum values of the horizontal electric field  $(Max(E_H))$  occurs along the Norwegian coast due to the well-known coastal effect (Gilbert, 2005) with values of 10 V/km up to  $\sim$  30 V/km. During this time interval, regions of Sweden distant from the north-west coast experienced  $E_H$  values around 2 V/km, with local maxima between 4 and 8 V/km in areas with strong conductivity gradients, and generally remaining below 1 V/km in regions of high conductivity.

The time series in Figure 2b,c shows that almost all locations experienced the maximum  $dB_H/dt = \sqrt{(dB_x/dt)^2 + (dB_y/dt)^2}$  at the moment of the abrupt weakening of the WEJ at 20:08:30 UT, with a maximum near 62° MLAT (violet line). The magnitude gradually decreases at higher latitudes and drops off more sharply toward lower latitudes. The peaks in  $E_H$  generally occur during periods of elevated  $dB_H/dt$ . However, the maximum values of  $E_H$  do not coincide exactly with the peaks in  $dB_H/dt$ . We notice that the time series around 60° MLAT (red line) presents relatively larger  $E_H$  values during the whole substorm.

The  $E_H$  maps during the evolution of the substorm is illustrated in the animation Case1\_BE.mp4 (panel e). In Sweden, large  $E_H$  values first appear in the north at the times when the WEJ peaks (19:55 UT), then shifts toward central Sweden by 19:58 UT, and reach lower latitudes near 20:04 UT (second WEJ peak), affecting a broad area of southern and central Sweden. Four minutes later, at 20:07:20 UT, the  $E_H$  maximum moves back to higher latitudes as the substorm evolves. Strong electric fields are again observed in central and southern Sweden around 20:08:50 UT, just after the WEJ weakening.

The  $E_H$  values were scaled to a 1-in-100 year event according to the MLAT bands presented in Table 2. The scaled  $E_H$  and the corresponding response in the Swedish power grid are illustrated in more detail in the animation Case1\_EGrid.mp4. In northern Sweden, where the scale factor is 1 (i.e., no scaling is applied), maximum  $E_H$  values reach only about 2 V/km.



180

185



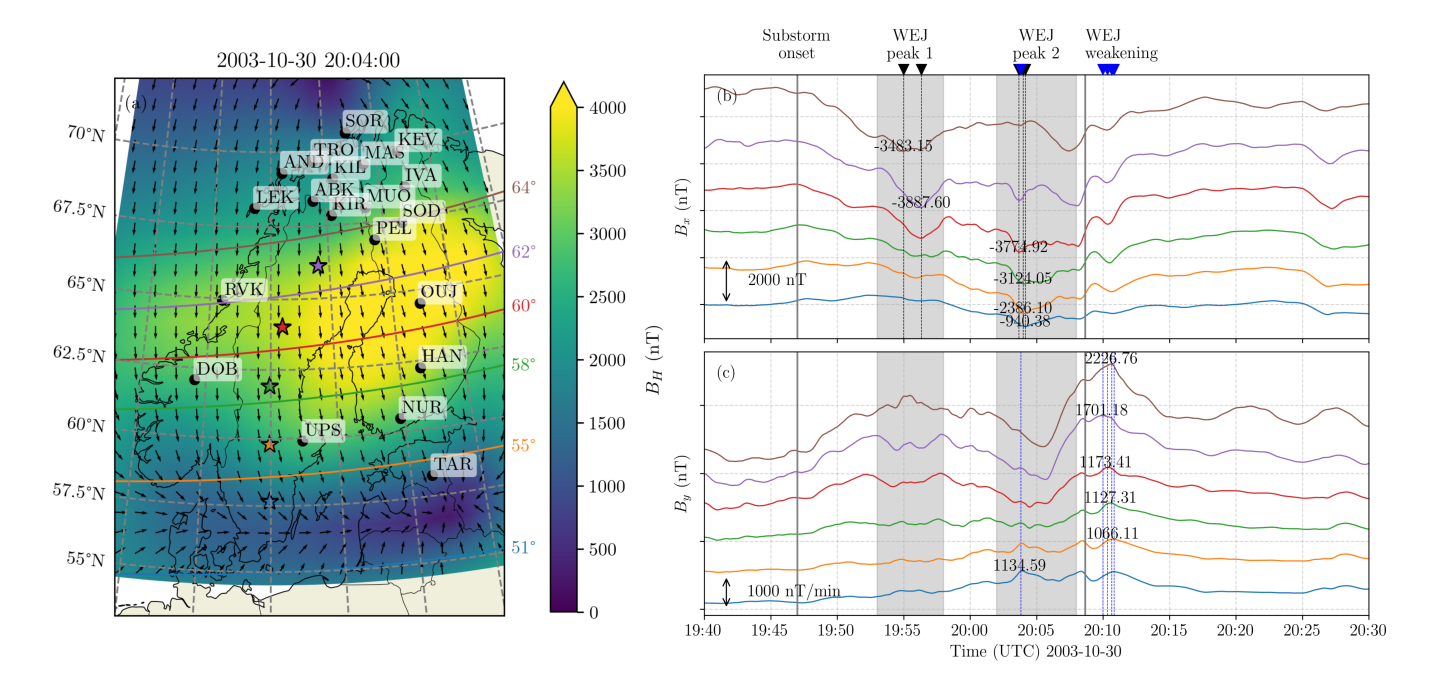


Figure 1. Ground magnetic field estimation during the 30 October 2003 geomagnetic storm. (a) Interpolated magnitude of the horizontal magnetic field  $(B_H)$  at 20:04 UT, the time when most stations recorded their maximum  $B_H$ . (b) Time series of the north-south  $\mathbf{B}$  component  $(B_x)$ , and (c) east-west  $\mathbf{B}$  component  $(B_y)$  at the locations indicated by a star in panel (a). The vertical black dashed lines indicate the  $B_x$  peaks, and the blue dashed lines indicate the peaks in  $B_y$ .

In contrast, southern and central Sweden show  $E_H$  about 2-6 V/km and 6-10 V/km respectively. The largest  $E_H$  values are observed between 55° and 58° MLAT, with values of around 6-10 V/km and a peak of approximately 12-15 V/km occurring in regions with strong conductivity gradients (Midskog, Töreboda, Söderhamn, Vittersjö, Göteborg). The maximum scaled  $E_H$  is summarized in Figure 6 and will be described in Section 4.

#### 3.2 Case 2: Simplified Uniform External Magnetic Field

In Case 2, we assume that a large ionospheric current is located over Fennoscandia. The ionospheric equivalent current shown in Figure 3a confirms that a strong current system was indeed present over northern and central Fennoscandia, with a maximum between Finland and Sweden. The right panel of Figure 3 shows  $B_{H,ext}$  and its time derivative at the magnetic stations around  $25.42^{\circ}$  E. This highlights the waveform variations across latitudes, showing similarities among the higher-latitude and, separately, among the lower-latitude, though with notable differences in amplitude. The maximum  $dB_{H,ext}/dt$  is observed almost simultaneously across all locations at 20:08:30, with a maximum near  $60^{\circ}$  MLAT (red line). The  $dB_{H,ext}/dt$  magnitude gradually decreases at higher latitudes and drops off more sharply toward lower latitudes. Due to the latitudinal differences in the waveforms, we had to determine which one was most representative of the current system to later apply it across the entire region. As a first approach, we selected the waveform from the OUJ station, as it was located near the center of the ionospheric



195



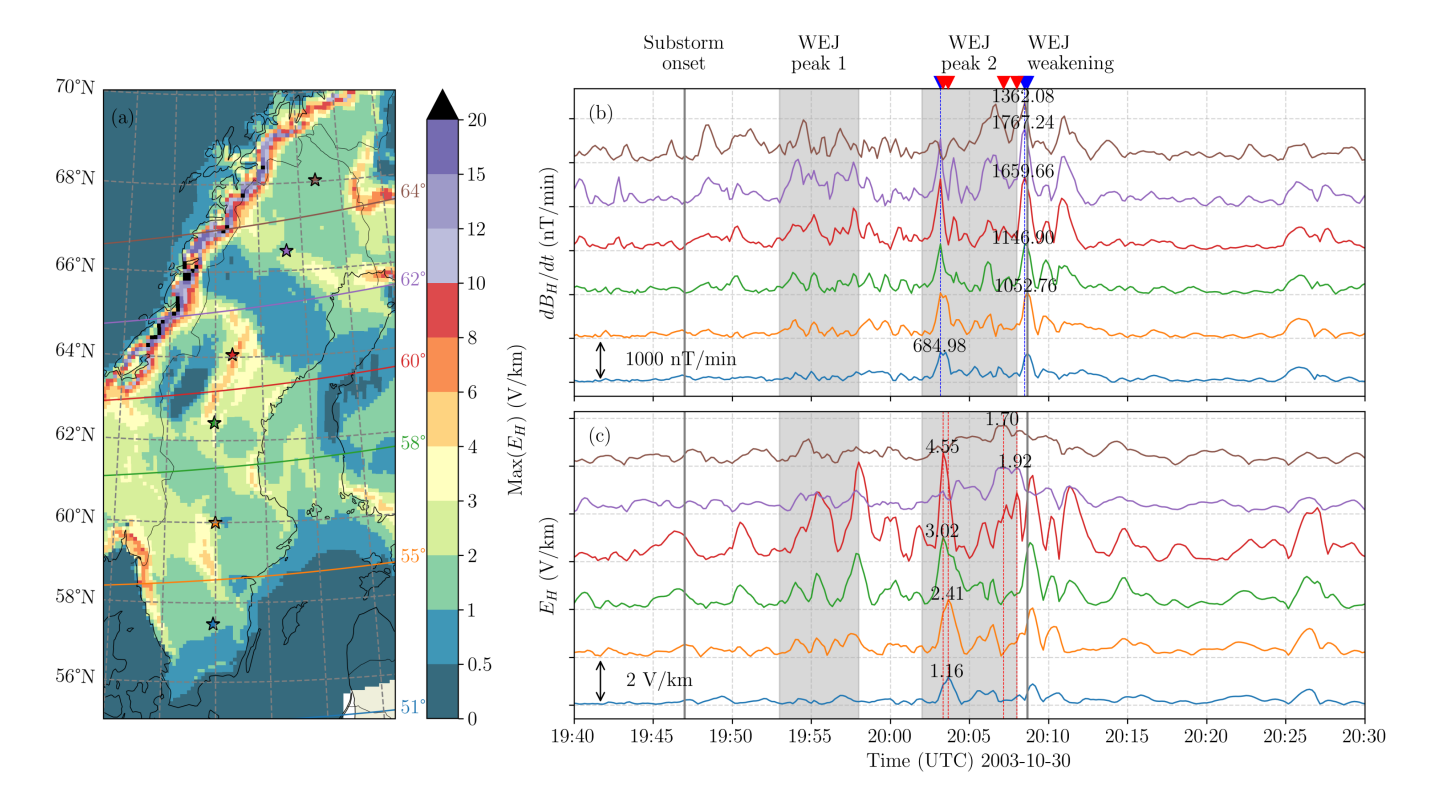


Figure 2. Case 1: Map of the maximum electric field magnitude during the interval 19:40–20:30 UT. The color scale indicates the peak electric field strength at each location. Colored stars mark specific sites where time series data were extracted, with the corresponding temporal  $dB_H/dt$  and  $E_H$  profiles shown in the panels (b) and (c) respectively. The vertical dashed lines indicate the moment of the series peak.

current and exhibited the largest  $dB_{H,ext}/dt$ . We also considered the magnetic field data from the HAN station, which showed a similar evolution but with a lower  $dB_{H,ext}/dt$ . Data from these two stations were used to compute the ground geoelectric field, and the waveform that produced the largest geoelectric field was selected.

The 3D electric field response in Sweden, computed using uniform magnetic field waveforms from OUJ and HAN ground-based stations as inputs, is shown in Figure 4. Differences in induced  $E_H$  at fixed positions are primarily driven by variations in the input  $B_{H,ext}$ . Although the OUJ and HAN stations exhibit similar  $B_{H,ext}$  waveforms (Figures 4a,d), the magnitude and perturbations are larger at OUJ; however, the induced electric field response is greater at HAN. This highlights how the geoelectric field is strongly influenced not only by the local ground conductivity but also by the frequency content of geomagnetic field variations. As shown in Dimmock et al. (2024, Figure 4), two distinct dH/dt peaks are observed around the time of the transformer trip event, yet the largest peak in the geoelectric field corresponds to the smaller of the two  $dB_H/dt$  peaks, further illustrating the non-linear and frequency-dependent nature of the relationship between magnetic and electric fields.



205

210



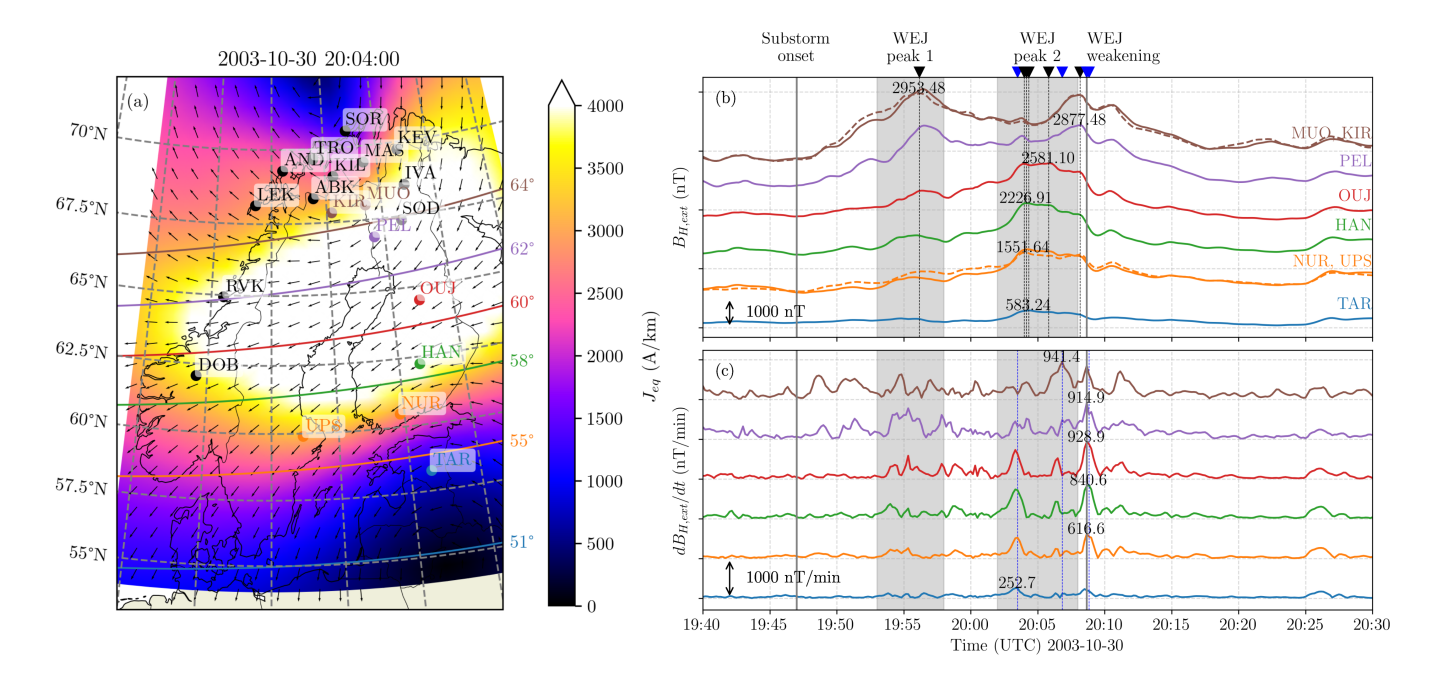


Figure 3. Ground-based estimations during the 30 October 2003 geomagnetic storm. (a) Ionospheric equivalent current  $(J_{eq})$  at 20:04 UT, the time when most stations recorded their maximum  $B_H$  and the  $J_{eq}$  reaches its minimum latitude. (b) Time series of the external part of the horizontal magnetic field magnitude  $(B_{H,ext})$ , and (c) Magnetic field perturbations  $(dB_{H,ext}/dt)$  at the magnetic stations along  $25.42^{\circ}$ E (solid line) and in Sweden (dashed line). The vertical black dashed lines indicate the  $B_H$  peaks, and the blue dashed lines indicate the peaks in  $dB_{H,ext}/dt$ .

For the scenario evaluated in this study, we chose the HAN station waveform, which resulted in the largest  $E_H$  response. However, we note that this is not a unique, but rather a representative selection for worst-case assessment. In the case of a spatially uniform magnetic field, the geoelectric field differences across the country purely depend on the ground conductivity. The time evolution of  $B_{H,ext}$ ,  $dB_{H,ext}/dt$  and  $E_H$  is shown in the animation Case2\_BE.mp4. The maximum  $E_H$  is detected around 20:09 UT, just after the  $dB_{H,ext}/dt$  peak, however the magnitude is smaller than Case 1 since we are evaluating the  $E_H$  from the external part of  $B_H$ . A second relative  $E_H$  maximum is detected at 20:03:40. As in Case 1, we scaled the  $E_H$  field values to be a once in 100-years events using the scaling factor in Table 2. The animation for the scaled  $E_H$  using HAN station waveform as input and the power line voltages are shown in Case2\_EGrid.mp4.

# 3.3 Comparison of Scaled $E_H$ between Case 1 and Case 2

A snapshot at the time of the scaled  $E_H$  peak (20:03:40 UT) for Case 1 and Case 2 are shown in Figure 5a,b, and the difference between both cases in Figure 5c. Above 62° MLAT, the largest differences are confined to the Norwegian coast, likely due to variations in the  $\boldsymbol{B}$  waveform at high latitudes between the two cases. In panels 5a,b, Case 1 shows southward-oriented  $\boldsymbol{E}$  on the seaside and landside of the Norwegian coast, while Case 2 exhibits eastward-oriented  $\boldsymbol{E}$  at both sides. Between  $58^\circ$  and





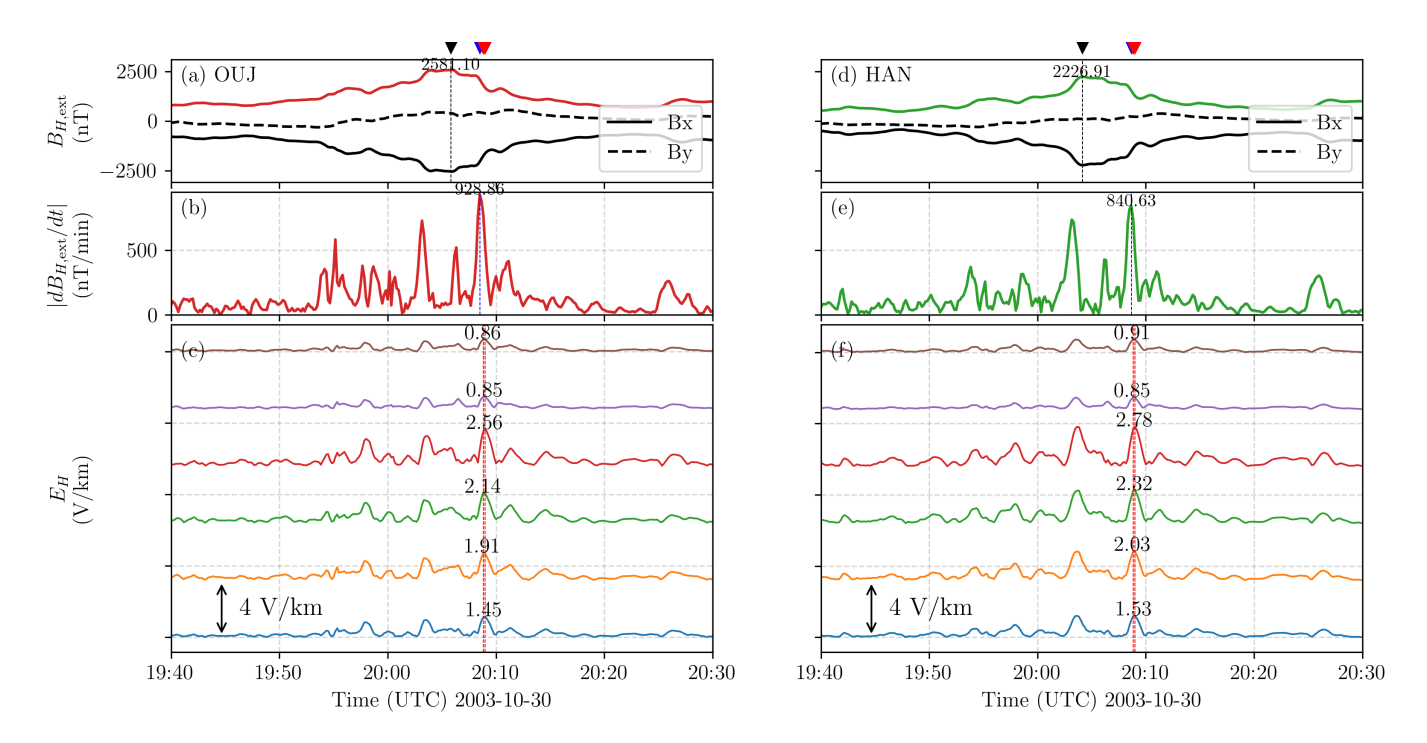


**Figure 4.** Case 2: Ground-based observations and estimated 3D geoelectric field during the 30 October 2003 geomagnetic storm. (a, d) Magnitude of the horizontal magnetic field observed by OUJ, and HAN stations respectively, (b, e) magnetic field perturbations, and (c, f) horizontal geoelectric field time series at fixed locations shown with stars in Figure 1a.

 $62^{\circ}$  MLAT, the differences are minimal since this range corresponds to the selected HAN station and the similarly response at the OUJ station. The remaining variations can be mainly attributed to the difference between  $B_{tot}$  and  $B_{ext}$ .

Below  $60^{\circ}$  MLAT, the differences become more evident. In the  $55-58^{\circ}$  MLAT band, both cases present the largest maximum scaled  $E_H$ , but for Case 1  $E_H$  is larger than in Case 2, particularly in the western region due to strong conductivity gradients, as well as along the east coast. In southern Sweden ( $51-55^{\circ}$  MLAT band), the scaled  $E_H$  values in Case 2 exceed those in Case 1 by about 4 V/km at the coasts. This difference is mainly related to the larger B magnitude and perturbations obtained in Case 2 compared to those derived from the B interpolation, which is strongly affected by the lack of magnetic field measurements in southern Sweden and relies primarily on interpolation from the TAR magnetic station.

### 4 Swedish power grid impacts

215

The impact on the Swedish power grid for the Case 1 worst-case scenario is summarized in Figure 6. The maximum scaled  $E_H$  between 19:40 UT and 20:30 UT reaches approximately 8 V/km in at least four regions: the southwest coast near Göteborg, the central east coast near Vittersjö, central Sweden near Midskog, and central Sweden near Karlstad. Around these areas, the power line voltage per km exceeded 3 V/km (red lines in Figure 6b). Power lines that exceeded 3 V/km are typically short



230

235



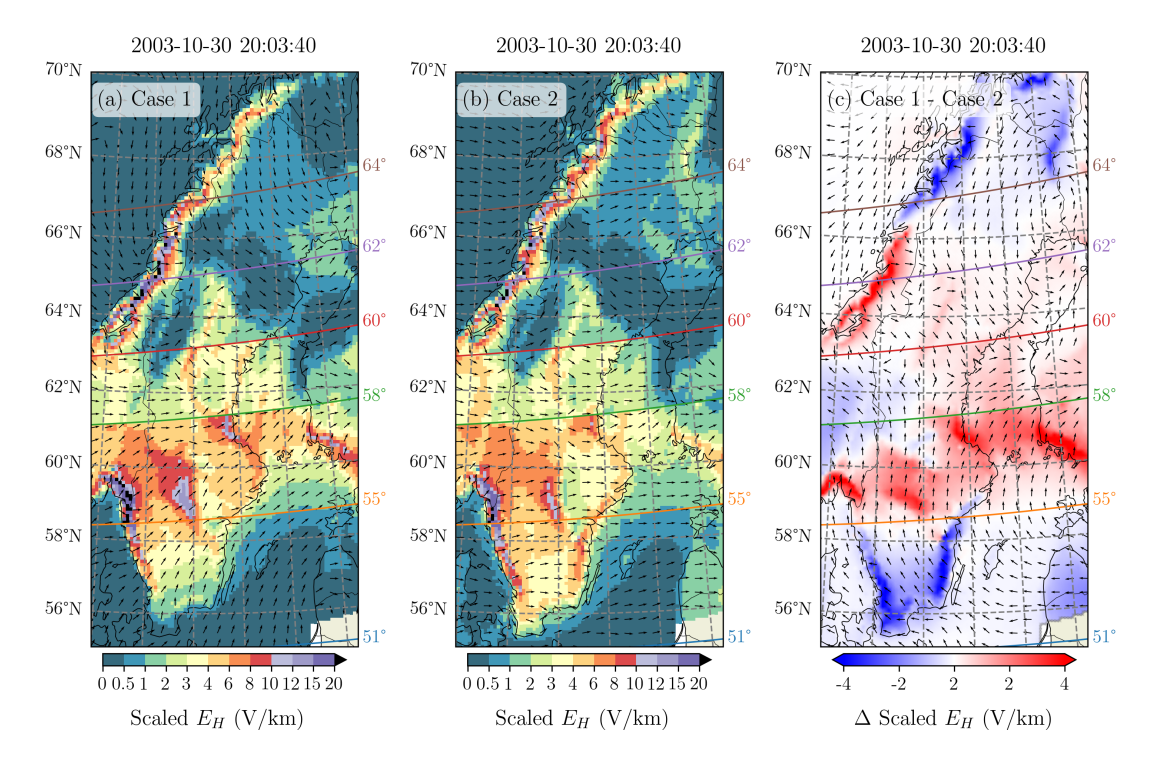


Figure 5. Comparison between the scaled  $E_H$  for Case 1 and Case 2. Panels (a) and (b) show the spatial distribution at 20:03:40 UT. Panel (c) Shows the difference of scaled  $E_H$  between Case 1 and Case 2.

east—west oriented, but some north—south oriented lines near regions of high  $E_H$  are also present (e.g., Vittersjö, and south-west Sweden). In contrast, power lines with voltages per km below 1 V/km throughout the storm (black lines) are mainly located in northern Sweden and at the far south, but notably, some are also found near the Stockholm area close to lines showing high voltages, highlighting the complexity of the system.

For Case 2, the maximum scaled  $E_H$  and resulting power line impacts differ from Case 1, particularly in southern Sweden, due to the larger  $E_H$  values in this region as previously discussed in Figure 5 and also evident from Figure 7a. Consequently, power lines exceeding 3 V/km appear even at lower latitudes in Figure 7e.

In both cases, the lines that did not exceed 1 V/km are primarily north–south oriented in central and southern Sweden, while in northern Sweden, lines of any orientation generally did not experience high voltages per km.

Östersund, Midskog, Bandsjö, Stöde, Ånge, Söderhamn, Vittersjö, Karlstad, Töreboda, and the Stockholm area have been previously identified as vulnerable to GIC impacts (Dimmock et al., 2024; Rosenqvist et al., 2025; Hapgood, 2019; Kappenman, 2006). Figures 6a and 7a show that these locations lie in close proximity to regions of elevated  $E_H$  in both worst-case scenarios. Their large  $E_H$  values appears to be linked to nearby zones of strong lateral conductivity gradients, which emerge as a critical risk factor. Interestingly, Malmö, which experienced a GIC-induced blackout in 2003, does not appear as a major hotspot in the Case 1 results. This may be attributed to the limited magnetometer coverage in southern Sweden (MLAT  $< 55^{\circ}$ )





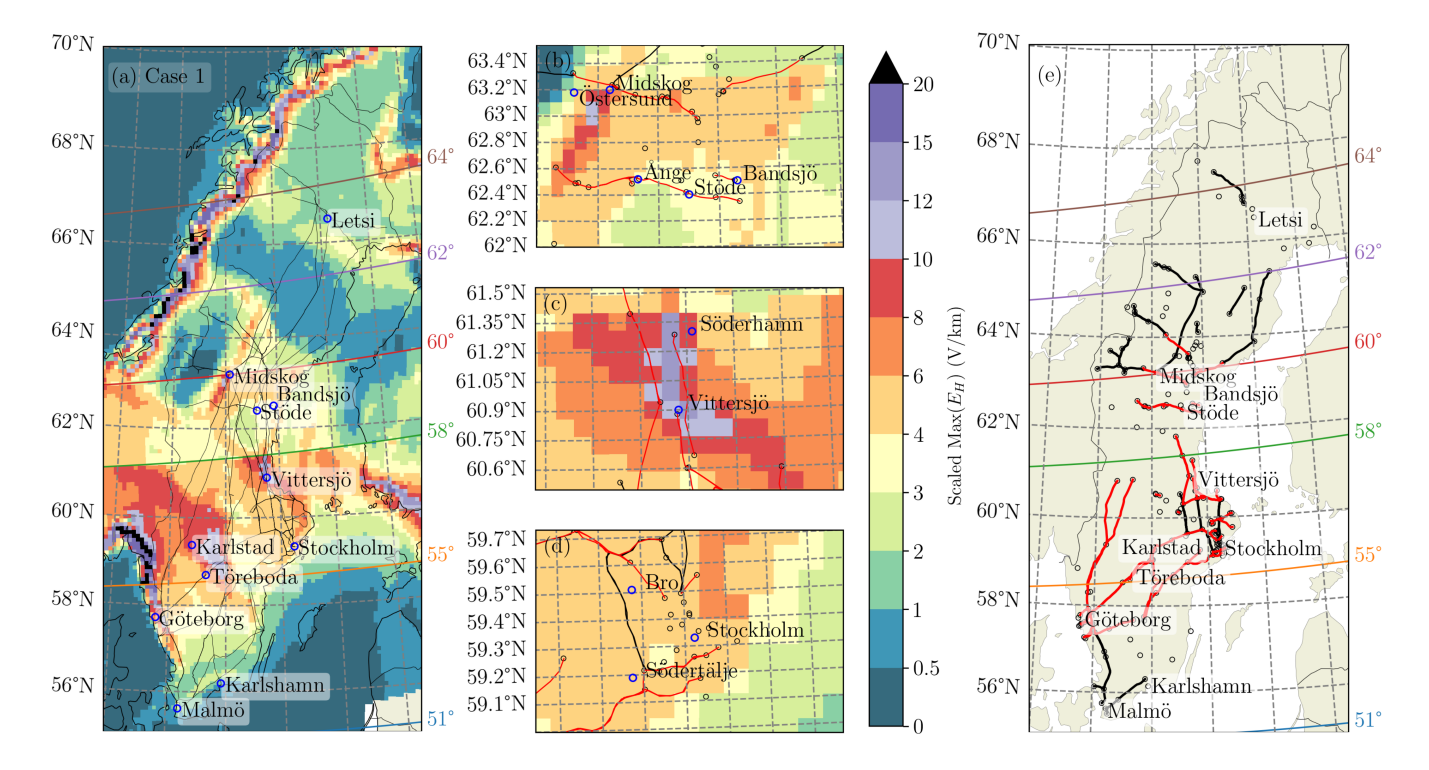


Figure 6. Case 1: (a) Maximum scaled  $E_H$  across Sweden during the period 19:40:00–20:30:00 UT on 30 October 2003. Panels (b), (c), and (d) show zoomed-in views for the Midskog, Vittersjö, and Stockholm regions, respectively. (e) Power lines that exceeded voltages per km 3 V/km (red), and power lines that remained below 1 V/km (black).

during the Halloween event. Notably, Malmö is identified as vulnerable under Case 2, when a large-scale ionospheric current system is assumed.

A particularly noteworthy case is Karlshamn, which appears susceptible to GICs even under relatively low  $E_H$  values, between 0.42 V/km and 0.75 V/km, according to Table 1 in (Rosenqvist et al., 2025). This highlights how local grid topology and substation characteristics may drive vulnerability independently of regional  $E_H$  strength. Another explanation could be that the ground conductivity might not be well represented here.

## 245 4.1 Comparison between Case 1 and Case2

For each line, we computed its orientation by assuming a straight line between its starting and ending geographic positions. This analysis shows that the network is largely north–south oriented, with 63% of the lines having angles greater than 45°, reflecting the country's elongated shape. East–west oriented lines (angles less than 45°) are mainly concentrated within the latitude band 58–64° N, which is also where most lines are located, as shown in Figure 6a.

The maximum voltage for each line during the two worst-case scenarios, categorized by its orientation, is summarized in Figure 8. Voltages are highest for north-south oriented lines, which are typically the longest. However, when normalized by line



260

265



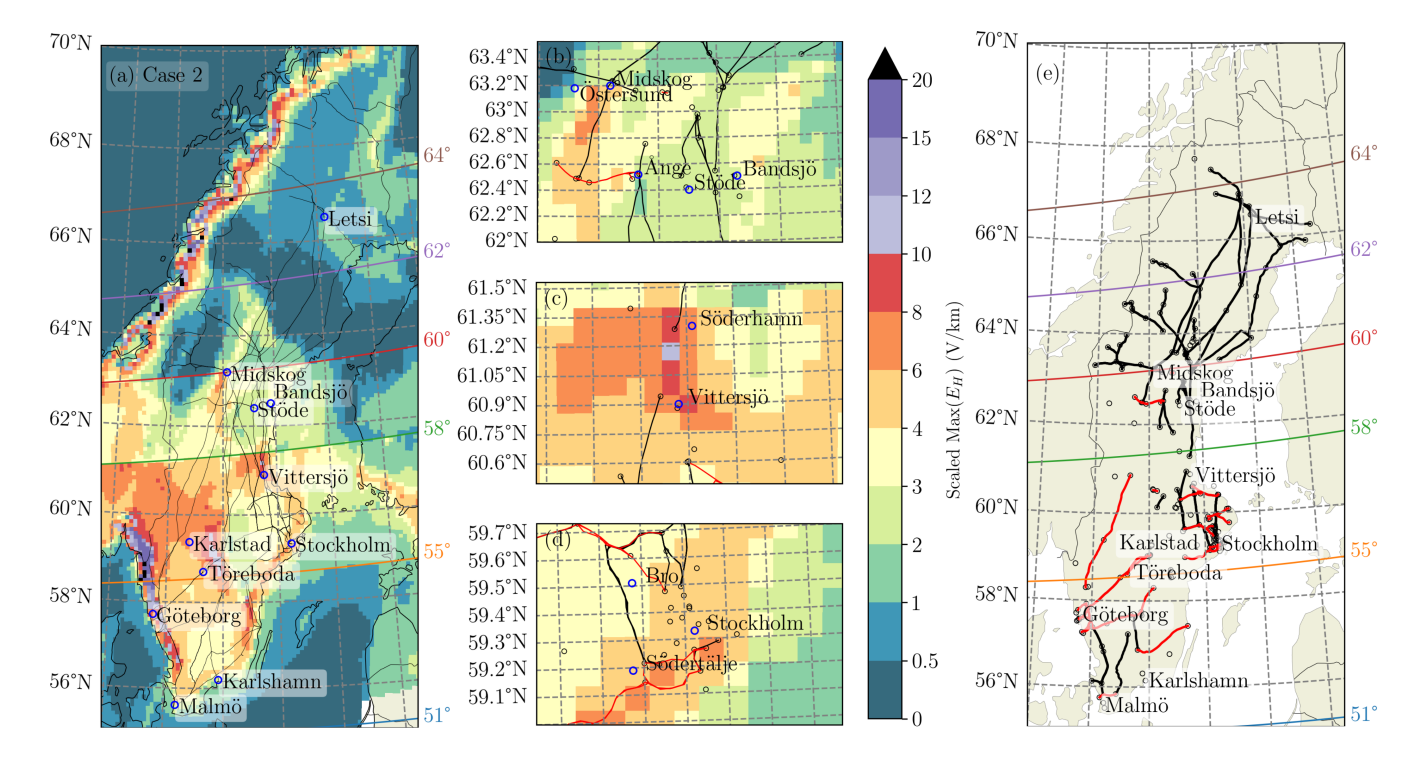


Figure 7. Same as Figure 6, but for Case 2. (a) Maximum scaled  $E_H$  across Sweden during the period 19:40:00–20:30:00 UT on 30 October 2003 and zoom-in views (b-c) around Midskog, Vittesjö and Stockholm. (e) Power lines that exceeded voltages per km 3 V/km (red), and power lines that remained below 1 V/km (black).

length, east—west oriented lines exhibit the largest values, ranging between 6–8 V/km due to the preferred east-west orientation of the  $E_H$  (specially for Case 2). In general, the voltage in the line increases with length as shown in Figure 8c. Lines shorter than 20 km did not reach the level of 100 V in either scenario, and voltages above 10 V begin to appear for lines longer than 2 km. The median length of the 335 transmission lines is 53 km. For lines longer than 50 km, 73% experience voltages above 100 V at least once in Case 1, and 60% in Case 2. These fractions decrease to 37% and 28%, respectively, when the threshold is raised to 200 V, which still represents a substantial number of affected lines.

Finally, for both worst-case scenarios, the number of power lines experiencing voltages exceeding 10 V easily exceeds 100 lines on more than 9 occasions during the analyzed period, while about 100 lines exceed 50 V at different stages of the substorm, as illustrated in Figure 9. Among these 100 lines, 16, 7, and 1 lines are connected near the main Swedish cities of Stockholm, Göteborg, and Malmö, respectively. At the moment of the WEJ weakening around 100 lines experienced voltages larger than 100 V. Of these, 6 lines were located near Stockholm and 7 near Göteborg, while no lines around Malmö exceeded the 100 V threshold. This worst case scenario raises a critical question not only about whether the power grid infrastructure can endure such widespread stress, but also whether system operators are sufficiently prepared to detect, manage, and respond to a situation involving not just a few, but potentially 100 affected lines, spanning multiple regions.





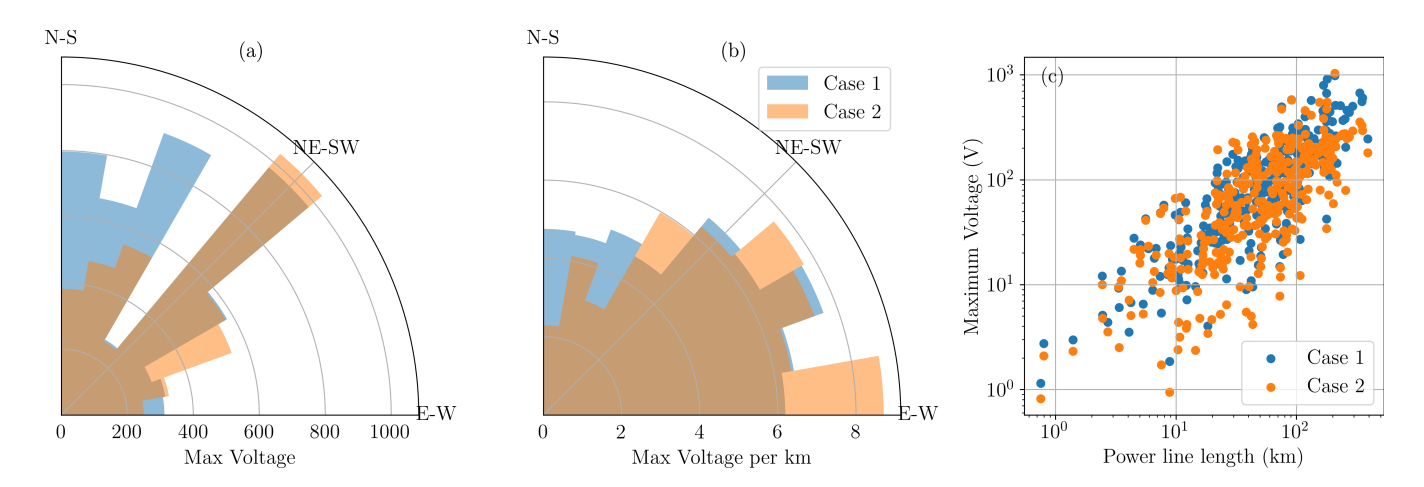


**Figure 8.** (a-b) Maximum voltage and voltage per km (V/km) by power line orientation. (c) Relation between the power line length and the maximum voltage reached for the Case 1 and Case 2 worst-case scenarios.

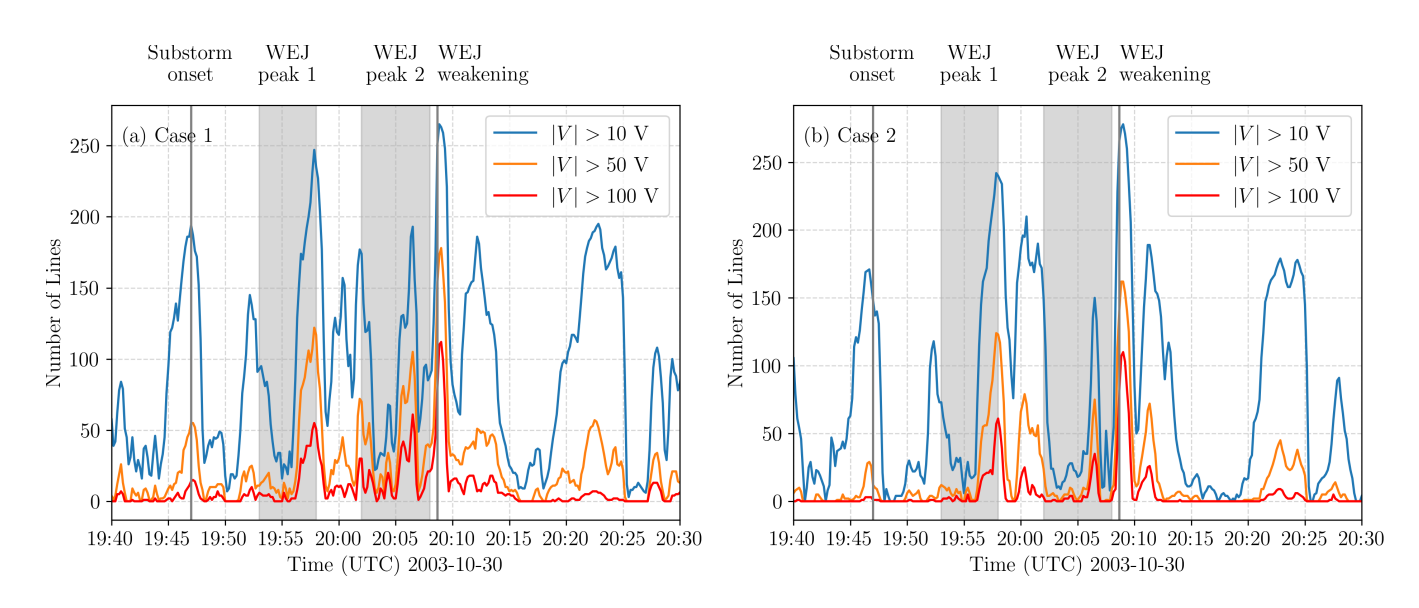


Figure 9. Number of lines exceeding Voltages |V| > 10 V (blue), |V| > 50 V (orange), and |V| > 100 V (red) for the worst-case scenarios (a) Case 1 and (b) Case 2.





#### 5 Discussion

275

280

285

290

295

This study presents the first assessment of a worst-case scenario for the entire Swedish power grid using real data in MLT sectors where the largest geomagnetic activity is known to occur. We applied the recently developed RAISE model (Rosenqvist et al., 2025) to evaluate the impacts of an extreme horizontal geoelectric field, representative of a 1-in-100-year event, on the Swedish power grid. To represent this extreme event, we derived the induced  $E_H$  from the 30 October 2003 Halloween geomagnetic storm between 19:40 to 20:30 UT and subsequently scaled it to a 1-in-100-year level using return periods reported in (Lanabere et al., 2024). We conducted the analysis following two different approaches, reflecting the fact that there is no exact definition of what constitutes an extreme event. From the perspective of scaling existing measurements, we identified two plausible options and aimed to explore both. This allowed us not only to evaluate the impacts under each assumption but also to assess the sensitivity of the results to the choice of approach. In Case 1, we used actual magnetic field observations across Fennoscandia to estimate the  $E_H$  in Sweden. This case accounts for the combined effect of regional magnetic field waveforms and spatial variations in ground conductivity. In Case 2, we assumed the presence of a large-scale ionospheric current system located over Fennoscandia, resulting in a spatially uniform magnetic field waveform across Sweden. Consequently, the variability in the  $E_H$  arises solely from differences in ground conductivity.

# 5.1 Maximum estimated and observed E values

In this study, the induced  $E_H$  for the Halloween event was scaled to represent a 1-in-100 year scenario. In particular, a scaling factor of three was used within the  $55-58^{\circ}$  MLAT band, representing a conservative lower bound. Based on the 95th percentile confidence interval of (Lanabere et al., 2024), the scaling could be as high as a factor of five. This implies our modeled scenario likely underestimates the potential severity, providing a lower limit benchmark for extreme conditions. Nonetheless, even under this conservative scaling, maximum  $E_H$  values reached approximately 10-12 V/km between  $55^{\circ}$  and  $58^{\circ}$  MLAT.

These values are consistent with estimates for the May 1921 storm, which exceeded the 1-in-100-year return level and caused catastrophic damage to the telegraph and telephone station at Karlstad, where geoelectric fields likely reached  $\sim 10$  V/km, as discussed by Hapgood (2019) and references therein. Hapgood (2019) also reports other impacts in Sweden: Östersund and Söderhamn experienced extremely powerful earth currents; Telephone lines between Göteborg and Stockholm were unstable and GIC measurements of about 1.1 Amp; a minor fire at the telegraph and phone station of Ånge. The suggested  $E_H = 10$ V/km in Karlstad discussed in Hapgood (2019) is close to the area of 10-12 V/km of the scaled  $E_H$  of both worst-case scenarios.

In the case of the 13-14 July 1982 storm, which was less intense than the Halloween event (Dst minimum of -325 nT), the voltage peak value in telecommunication cable between Södertälje-Stockholm and Bro-Stockholm was roughly 80 V, implying an estimated east—west-oriented electric fields of approximately 4-5 V/km (Wik et al., 2009). In Figures 6e and 7e, a power line in Södertälje appears in the lines exceeding Voltages per km > 3 V/km. However, during the 1982 event, highly localized electric fields of up to 9.1 V/km were inferred from observations along a short 921 m segment of the 100 km railway



300

305

325

330



communication line between Stockholm and Töreboda (Kappenman, 2006). Notably, Töreboda lies within the  $55-58^{\circ}$  MLAT band, crosses a region with strong conductivity gradients, and the  $E_H$  values in both cases exceeds 10 V/km.

In the reference study by Pulkkinen et al. (2012), maximum  $E_H$  values of 20 V/km were assumed for resistive ground structures above the MLAT threshold and 5 V/km below it, while for conductive ground structures the corresponding values were 2 V/km and 0.5 V/km. In our analysis, we find scaled  $E_H$  values exceeding 20 V/km in highly localized regions near the west coast. However, the choice of 2 V/km for conductive ground areas above the MLAT threshold in Pulkkinen et al. (2012) appears somewhat higher than our estimates, which range between 0.5 and 1 V/km. Below the MLAT threshold, their maximum values for resistive ground (5 V/km) are consistent with our results, where we obtain maximums of 4 to 6 V/km. For the 0.5 V/km limit in conductive areas below the MLAT threshold, no direct comparison with our analysis is possible.

### 5.2 Power grid implications

To prevent permanent transformer damage from GICs, the Swedish power grid requires that new transformers withstand a direct current of 200 A for 10 minutes while operating at full load (private communication with Johan Setréus, Svenska Kraftnät). Since the actual line resistances are considered sensitive information, we adopted a constant ground resistance of  $R_{GR} = 0.5$ ,  $\Omega$  and line resistances of  $R_{L,220} = 0.022$ ,  $\Omega$  and  $R_{L,400} = 0.008$ ,  $\Omega$ , following the values used by Viljanen et al. (2012). Based on these assumptions, we find that GICs of 200 A can be reached even in short (< 20 km) 220 kV and 400 kV lines under a  $E \sim 10$  V/km oriented parallel to the line. However, such large E values, and consequently large currents, typically occur only in very short bursts rather than being sustained. The 10-minute requirement is also ambiguous: it is unclear whether it refers to continuous or cumulative current exposure. Moreover, this specification applies only to the newest transformers, and no information is available for the tolerances of different units. These results are important since they show that the 200 A limit can be reached, however a future study will be required to determine the impact on Swedish transformers.

Although past extreme space weather events have been linked to permanent transformer damage, the simultaneous tripping of a large number of transformers also represents a serious worst-case scenario. In our study, we find that during the peak and subsequent weakening of the WEJ, large dB/dt and  $E_H$  values were estimated at latitudes below  $60^{\circ}$  MLAT. As a consequence, approximately 100 power lines experienced induced voltages exceeding 50 V at several times during the substorm period. Of these, 16 were located near the capital city, Stockholm, and seven near Göteborg, Sweden's second most populated city. During the weakening phase of the WEJ, estimated voltages reached up to 100 V on about 100 lines, including six in the Stockholm area and seven in the Göteborg area. For comparison, Lucas et al. (2018) reported that 62 transmission lines exceeded 100 V during the March 1989 geomagnetic storm, which triggered a major blackout in the Hydro-Québec power system. The large number of power lines subjected to high induced voltages in our scenario could pose a significant risk to protection relays, potentially leading to widespread and unnecessary tripping of both lines and transformers. Such widespread disconnections could result in power-loss and inevitable socioeconomic impacts. Nevertheless, the relationship between induced voltages and the likelihood of unnecessary tripping remains uncertain in Sweden and further work will focus on better understanding this.



335



# 5.3 Future implications

This study builds on a series of investigations in Sweden that have significantly advanced understanding of induced electric fields and the power grid's response to geomagnetic activity (e.g., Wik et al., 2008; Wik et al., 2009; Wintoft et al., 2016; Dimmock et al., 2019; Rosenqvist and Hall, 2019; Rosenqvist et al., 2022; Lanabere et al., 2023; Lanabere et al., 2024; Dimmock et al., 2024; Rosenqvist et al., 2025; Wallner et al., manuscript submitted). Expanding on this foundation, we provide the first detailed and comprehensive assessment of the potential impacts of a 1-in-100-year ground electric field on the Swedish power grid. Importantly, our analysis is based on total voltage, representing the geoelectric field integrated along each line's path. Because information on individual line resistances is not available, we could not convert voltages into GICs. Future versions of the RAISE model may incorporate this capability.

The main goal of this study is to benchmark a severe geoelectric field event and understand how it could affect the power grid, given the known layout. This has provided meaningful insights into regions that may be at risk. We also assessed the number of lines that could be subjected to hazardous GICs during a 1-100 year event. An added benefit of this work is that Svenska Kraftnät can use this knowledge for their own investigations using realistic grid configurations. We view this work as a significant advancement for Sweden in understanding the effects of rare, high-impact events.

Nevertheless, there are still many unanswered questions to address, such as the following: (1) How do small-scale ionospheric currents during extreme storms influence the spatial variability of geoelectric fields and GICs? (2) Is the current number of magnetometers sufficient to adequately capture space weather impacts in low MLAT regions, particularly in areas of large conductivity gradients? (3) Are power grid operators equipped and prepared to manage simultaneously high induced voltages occurring on multiple power lines during extreme geomagnetic storms? Our aim is to continue to address these key questions in future studies.

#### 6 Conclusions

355

We used the recently developed RAISE model (Rosenqvist et al., 2025) to investigate the impacts in the Swedish power grid during a 1-in-100 year geoelectric field event. The main findings from this study are summarized as follows:

- 1. The largest scaled  $E_H$  are found within the 55°-58° MLAT band, reaching up to  $\sim$ 12 V/km, particularly in regions with strong lateral conductivity gradients.
- 2. East-west-oriented power lines below 60° MLAT are generally more susceptible to large induced voltages due to the prevailing orientation of the horizontal electric field.
- 3. Voltage per km larger than 3 V/km are concentrated near substations that have historically reported GIC disturbances, including Midskog, Bandsjö, Vittersjö, and the Stockholm area.



370



- 4. In western Sweden, several power lines exhibit voltage per km larger than 3 V/km even when oriented northwest–southeast, primarily due to localized conductivity structures. In eastern Sweden the power lines exceeding 3 V/km between Vittersjö and Söderhamn are oriented north-south along an area of extremely large E<sub>H</sub> values.
  - 5. Interestingly, the Karlshamn substation, identified in previous studies as GIC-prone, does not exhibit high  $E_H$  levels, even when assuming a uniform ionospheric current system.
- 6. The lack of strong responses in Malmö, despite its documented blackout in 2003, is likely due to limited magnetometer coverage in southern Sweden (MLAT < 55°), which may lead to underestimated impacts in this region under real conditions.
  - 7. During the WEJ peaks and sudden weakening of worst-case scenarios, around 100 power lines experienced voltages larger than 50 V several times during the substorm, and about 100 lines exceeded 100 V at the moment of the WEJ weakening, which occurs close to the time of maximum  $dB_H/dt$ .

Code and data availability. IMAGE data is available at the website https://space.fmi.fi/image/. A code for the SECS analysis is available in (Vanhamäki and Juusola, 2020). The SMAP model conductivity profiles of Fennoscandia and their derivation can be found in the following manuscripts: Korja et al. (2002) and (Engels et al., 2002).

Video supplement. The videos in the Supplement illustrate the time evolution of the ground magnetic field produced by the ionospheric equivalent current, the induced 3D geoelectric field, the scaled 3D geoelectric field, and the voltage in the power lines for Case 1 and Case 2 on 30 October 2003, from 19:40:00 to 20:30:00 UT (50 min), with a 10 s time step. The animations consist of frames similar to those shown in Fig. 1, Fig. 2 and Fig. 5a,b.

Author contributions. V.L prepared the material and wrote the manuscript together with A.D and S.M. A.W provided expertise on GICs, S.M, L.R, and A.J on the RAISE model. J.S on power grid operations. All coauthors read the manuscript and commented on it.

380 *Competing interests.* The authors declare that they have no conflict of interest.

Acknowledgements. V. L., A. P. D., L. R, A. J., and S. M were funded by the Swedish Research Council project grant 51128 VR 2021-06259. A. P. D. received support from the Swedish National Space Agency (Grant 2020-00111). We thank the institutes who maintain the IMAGE Magnetometer Array: Tromsø Geophysical Observatory of UiT the Arctic University of Norway (Norway), Finnish Meteorological Institute (Finland), Institute of Geophysics Polish Academy of Sciences (Poland), GFZ German Research Centre for Geosciences (Germany),





Geological Survey of Sweden (Sweden), Swedish Institute of Space Physics (Sweden), Sodankylä Geophysical Observatory of the University of Oulu (Finland), Polar Geophysical Institute (Russia), DTU Technical University of Denmark (Denmark), and Science Institute of the University of Iceland (Iceland). The provisioning of data from AAL, GOT, HAS, NRA, VXJ, FKP, ROE, BFE, BOR, HOV, SCO, KUL, and NAQ is supported by the ESA contracts number 4000128139/19/D/CT as well as 4000138064/22/D/KS.





#### References

395

405

- 390 Amm, O.: Ionospheric Elementary Current Systems in Spherical Coordinates and Their Application, Journal of geomagnetism and geoelectricity, 49, 947–955, https://doi.org/10.5636/jgg.49.947, 1997.
  - Amm, O. and Viljanen, A.: Ionospheric disturbance magnetic field continuation from the ground to the ionosphere using spherical elementary current systems, Earth, Planets and Space, 51, 431–440, https://doi.org/10.1186/BF03352247, 1999.
  - Bergin, A., Chapman, S. C., Watkins, N. W., Moloney, N. R., and Gjerloev, J. W.: Extreme Event Statistics in Dst, SYM-H, and SMR Geomagnetic Indices, Space Weather, 21, e2022SW003304, https://doi.org/10.1029/2022SW003304, 2023.
  - Bolduc, L.: GIC observations and studies in the Hydro-Québec power system, Journal of Atmospheric and Solar-Terrestrial Physics, 64, 1793–1802, https://doi.org/10.1016/S1364-6826(02)00128-1, 2002.
  - Carrington, R. C.: Description of a Singular Appearance seen in the Sun on September 1, 1859, Monthly Notices of the Royal Astronomical Society, 20, 13–15, https://doi.org/10.1093/mnras/20.1.13, 1859.
- Cordell, D., Mann, I. R., Dimitrakoudis, S., Parry, H., and Unsworth, M. J.: Long-Term Peak Geoelectric Field Behavior for Space Weather Hazard Assessment in Alberta, Canada Using Geomagnetic and Magnetotelluric Measurements, Space Weather, 23, e2024SW004305, https://doi.org/https://doi.org/10.1029/2024SW004305, 2025.
  - Dimmock, A. P., Rosenqvist, L., Hall, J.-O., Viljanen, A., Yordanova, E., Honkonen, I., André, M., and Sjöberg, E. C.: The GIC and Geomagnetic Response Over Fennoscandia to the 7–8 September 2017 Geomagnetic Storm, Space Weather, 17, 989–1010, https://doi.org/10.1029/2018SW002132, 2019.
  - Dimmock, A. P., Lanabere, V., Johlander, A., Rosenqvist, L., Yordanova, E., Buchert, S., Molenkamp, S., and Setréus, J.: Investigating the Trip of a Transformer in Sweden During the 24 April 2023 Storm, Space Weather, 22, e2024SW003948, https://doi.org/https://doi.org/10.1029/2024SW003948, 2024.
- Engels, M., Korja, T., and the BEAR Working Group: Multisheet modelling of the electrical conductivity structure in the Fennoscandian Shield, Earth, Planets and Space, 54, 559–573, https://doi.org/10.1186/BF03353045, 2002.
  - Gilbert, J. L.: Modeling the effect of the ocean-land interface on induced electric fields during geomagnetic storms, Space Weather, 3, https://doi.org/https://doi.org/10.1029/2004SW000120, 2005.
  - Hapgood, M.: The Great Storm of May 1921: An Exemplar of a Dangerous Space Weather Event, Space Weather, 17, 950–975, https://doi.org/10.1029/2019SW002195, 2019.
- Juusola, L., Vanhamäki, H., Viljanen, A., and Smirnov, M.: Induced currents due to 3D ground conductivity play a major role in the interpretation of geomagnetic variations, Annales Geophysicae, 38, 983–998, https://doi.org/10.5194/angeo-38-983-2020, 2020.
  - Juusola, L., Viljanen, A., Dimmock, A. P., Kellinsalmi, M., Schillings, A., and Weygand, J. M.: Drivers of rapid geomagnetic variations at high latitudes, Annales Geophysicae, 41, 13–37, https://doi.org/10.5194/angeo-41-13-2023, 2023.
- Kappenman, J. G.: Great geomagnetic storms and extreme impulsive geomagnetic field disturbance events An anal-420 ysis of observational evidence including the great storm of May 1921, Advances in Space Research, 38, 188–199, https://doi.org/https://doi.org/10.1016/j.asr.2005.08.055, the Great Historical Geomagnetic Storm of 1859: A Modern Look, 2006.
  - Kataoka, R. and Ngwira, C.: Extreme geomagnetically induced currents, Progress in Earth and Planetary Science, 3, 23, https://doi.org/10.1186/s40645-016-0101-x, 2016.





- Korja, T., Engels, M., Zhamaletdinov, A. A., Kovtun, A. A., Palshin, N. A., Smirnov, M. Y., Tokarev, A. D., Asming, V. E., Vanyan, L. L.,
  Vardaniants, I. L., and Group, B. W.: Crustal conductivity in Fennoscandia—a compilation of a database on crustal conductance in the Fennoscandian Shield, Earth, Planets and Space, 54, 535–558, https://doi.org/10.1186/BF03353044, 2002.
  - Lanabere, V., Dimmock, A. P., Rosenqvist, L., Juusola, L., Viljanen, A., Johlander, A., and Odelstad, E.: Analysis of the Geoelectric Field in Sweden Over Solar Cycles 23 and 24: Spatial and Temporal Variability During Strong GIC Events, Space Weather, 21, e2023SW003588, https://doi.org/https://doi.org/10.1029/2023SW003588, 2023.
- 430 Lanabere, V., Dimmock, A. P., Rosenqvist, L., Viljanen, A., Juusola, L., and Johlander, A.: Characterizing the distribution of extreme geoelectric field events in Sweden, Journal of Space Weather and Space Climate, 14, 22, https://doi.org/10.1051/swsc/2024025, 2024.
  - Love, J. J., Rigler, E. J., Hayakawa, H., and Mursula, K.: On the uncertain intensity estimate of the 1859 Carrington storm, Journal of Space Weather and Space Climate, 14, 21, https://doi.org/10.1051/swsc/2024015, 2024.
- Lucas, G. M., Love, J. J., and Kelbert, A.: Calculation of Voltages in Electric Power Transmission Lines During Historic Geomagnetic Storms: An Investigation Using Realistic Earth Impedances, Space Weather, 16, 185–195, https://doi.org/10.1002/2017SW001779, 2018.
  - Mac Manus, D. H., Rodger, C. J., Dalzell, M., Renton, A., Richardson, G. S., Petersen, T., and Clilverd, M. A.: Geomagnetically Induced Current Modeling in New Zealand: Extreme Storm Analysis Using Multiple Disturbance Scenarios and Industry Provided Hazard Magnitudes, Space Weather, 20, e2022SW003 320, https://doi.org/10.1029/2022SW003320, 2022.
- Malone-Leigh, J., Campanyà, J., Gallagher, P. T., Hodgson, J., and Hogg, C.: Mapping Geoelectric Field Hazards in Ireland, Space Weather, 22, e2023SW003 638, https://doi.org/10.1029/2023SW003638, 2024.
  - NERC: Benchmark Geomagnetic Disturbance Event Description, Tech. rep., North American Electric Reliability Corporation, https://www.nerc.com/comm/OC/GeomagneticDisturbanceTaskForceGMDTF/Benchmark\_GMD\_Event\_Description\_Final.pdf, accessed: 2025-06-30, 2016.
- Ngwira, C. M., Pulkkinen, A., Wilder, V., and Crowley, G.: Extended study of extreme geoelectric field event scenarios for geomagnetically induced current applications, Space Weather, 11, 121–131, https://doi.org/https://doi.org/10.1002/swe.20021, 2013.
  - Pulkkinen, A., Lindahl, S., Viljanen, A., and Pirjola, R.: Geomagnetic storm of 29–31 October 2003: Geomagnetically induced currents and their relation to problems in the Swedish high-voltage power transmission system, Space Weather, 3, https://doi.org/10.1029/2004SW000123, 2005.
- Pulkkinen, A., Bernabeu, E., Eichner, J., Beggan, C., and Thomson, A. W. P.: Generation of 100-year geomagnetically induced current scenarios, Space Weather, 10, https://doi.org/https://doi.org/10.1029/2011SW000750, 2012.
  - Pulkkinen, A., Bernabeu, E., Thomson, A., Viljanen, A., Pirjola, R., Boteler, D., Eichner, J., Cilliers, P. J., Welling, D., Savani, N. P., Weigel, R. S., Love, J. J., Balch, C., Ngwira, C. M., Crowley, G., Schultz, A., Kataoka, R., Anderson, B., Fugate, D., Simpson, J. J., and MacAlester, M.: Geomagnetically induced currents: Science, engineering, and applications readiness, Space Weather, 15, 828–856, https://doi.org/10.1002/2016SW001501, 2017.
- Rosenqvist, L. and Hall, J. O.: Regional 3-D Modeling and Verification of Geomagnetically Induced Currents in Sweden, Space Weather, 17, 27–36, https://doi.org/10.1029/2018SW002084, 2019.
  - Rosenqvist, L., Fristedt, T., Dimmock, A. P., Davidsson, P., Fridström, R., Hall, J. O., Hesslow, L., Kjäll, J., Smirnov, M. Y., Welling, D., and Wintoft, P.: 3D Modeling of Geomagnetically Induced Currents in Sweden—Validation and Extreme Event Analysis, Space Weather, 20, e2021SW002988, https://doi.org/10.1029/2021SW002988, 2022.
- Rosenqvist, L., Johlander, A., Molenkamp, S., Dimmock, A. P., Setréus, J., and Lanabere, V.: A Novel Approach for Evaluating GIC Impacts in the Swedish Power Grid, Space Weather, 23, e2024SW004313, https://doi.org/https://doi.org/10.1029/2024SW004313, 2025.



475

480

485



- Siscoe, G., Crooker, N., and Clauer, C.: Dst of the Carrington storm of 1859, Advances in Space Research, 38, 173–179, https://doi.org/https://doi.org/10.1016/j.asr.2005.02.102, the Great Historical Geomagnetic Storm of 1859: A Modern Look, 2006.
- Thomson, A. W. P., Dawson, E. B., and Reay, S. J.: Quantifying extreme behavior in geomagnetic activity, Space Weather, 9, https://doi.org/https://doi.org/10.1029/2011SW000696, 2011.
  - Tsubouchi, K. and Omura, Y.: Long-term occurrence probabilities of intense geomagnetic storm events, Space Weather, 5, https://doi.org/https://doi.org/10.1029/2007SW000329, 2007.
  - Tsurutani, B. T., Gonzalez, W. D., Lakhina, G. S., and Alex, S.: The extreme magnetic storm of 1–2 September 1859, Journal of Geophysical Research: Space Physics, 108, https://doi.org/https://doi.org/10.1029/2002JA009504, 2003.
- Vanhamäki, H. and Juusola, L.: Correction to: Introduction to Spherical Elementary Current Systems, pp. C1–C1, Springer International Publishing, Cham, ISBN 978-3-030-26732-2, https://doi.org/10.1007/978-3-030-26732-2\_13, 2020.
  - Viljanen, A., Nevanlinna, H., Pajunpää, K., and Pulkkinen, A.: Time derivative of the horizontal geomagnetic field as an activity indicator, Annales Geophysicae, 19, 1107–1118, https://doi.org/10.5194/angeo-19-1107-2001, 2001.
  - Viljanen, A., Tanskanen, E. I., and Pulkkinen, A.: Relation between substorm characteristics and rapid temporal variations of the ground magnetic field, Annales Geophysicae, 24, 725–733, https://doi.org/10.5194/angeo-24-725-2006, 2006.
  - Viljanen, A., Pirjola, R., Wik, M., Ádám, A., Prácser, E., Sakharov, Y., and Katkalov, J.: Continental scale modelling of geomagnetically induced currents, Journal of Space Weather and Space Climate, 2, A17, https://doi.org/10.1051/swsc/2012017, 2012.
  - Wallner, A., Dimmock, A. P., Lanabere, V., Johlander, A., Molenkamp, S., Rosenqvist, L., Yordanova, E., Buchert, S., Juusola, L., Viljanen, A., Heiter, U., and Khotyaintsev, Y.: Investigating the geomagnetic storm on May 10-12 2024 and its effect on the Swedish power grid, Space Weather, manuscript submitted.
  - Wik, M., Viljanen, A., Pirjola, R., Pulkkinen, A., Wintoft, P., and Lundstedt, H.: Calculation of geomagnetically induced currents in the 400 kV power grid in southern Sweden, Space Weather, 6, 07005, https://doi.org/DOI: 10.1029/2007SW000343, 2008.
  - Wik, M., Pirjola, R., Lundstedt, H., Viljanen, A., Wintoft, P., and Pulkkinen, A.: Space weather events in July 1982 and October 2003 and the effects of geomagnetically induced currents on Swedish technical systems, Annales Geophysicae, 27, 1775–1787, https://doi.org/DOI: 10.5194/angeo-27-1775-2009, 2009.
  - Wintoft, P., Viljanen, A., and Wik, M.: Extreme value analysis of the time derivative of the horizontal magnetic field and computed electric field, Annales Geophysicae, 34, 485–491, https://doi.org/DOI: 10.5194/angeo-34-485-2016, 2016.